ACS APPLIED MATERIALS & INTERFACES

Research Article

www.acsami.org

Two-Dimensional, Porous Nickel–Cobalt Sulfide for High-Performance Asymmetric Supercapacitors

Xiaoming Li,[†,‡,§] Qiguang Li,[†,§] Ye Wu,[†] Muchen Rui,[†] and Haibo Zeng*[,†,‡]

[†]Institute of Optoelectronics & Nanomaterials, College of Material Science and Engineering, Nanjing University of Science and Technology, Nanjing 210094, China

[‡]State Key Laboratory of Mechanics and Control of Mechanical Structures and College of Materials Science and Technology, Nanjing University of Aeronautics and Astronautics, Nanjing 210016, China

Supporting Information

ABSTRACT: High specific surface area, high electrical conductivity, and abundant channels have been recognized to favor pseudocapacitors, but their realization at the same time is still a great challenge. Here, we report on nickel–cobalt sulfide nanosheets (NSs) with both ultrathin thickness and nanoscale pores for supercapacitors. The porous Ni–Co sulfide NSs were facilely synthesized through micelle-confined growth and subsequent sulfuration. The NSs are as thin as several nanometers and have a large number of pores with a mean size of ∼7 nm, resulting in ultrahigh atom ratio at surface with unique chemical and electronic structure. Therefore, fast diffusion of ions, facile transportation of electrons and high activity make great synergistic contributions to the surface-dependent reversible redox reactions. In the resulted supercapacitors, a specific capacitance of 1304 F g^{-1} is achieved at a current density of 2 A g^{-1} with excellent rate capability that 85.6% of the original capacitance is remained at 20 A g^{-1}. The effects of crystallinity and self-doping are optimized so that 93.5% of the original capacitance is obtained after 6000 cycles at a high current density of 8 A g^{-1}. Finally, asymmetric supercapacitors with a high energy density of 41.4 Wh/kg are achieved at a power density of 414 W/kg.

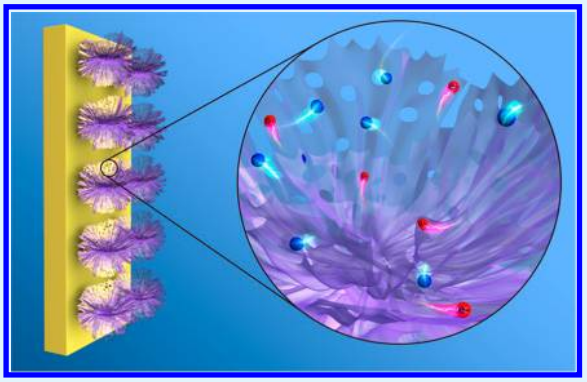

KEYWORDS: *ultrathin nanosheets, nickel–cobalt sulfide, crystallinity, self-doping, asymmetric supercapaitors*

INTRODUCTION

Recent reports on pseudocapacitors have demonstrated this kind of device to be excellent energy storage equipment for electric vehicles.[1−3] Their primary advantages lie in the fact that they have high power density and good cycling stability.[1−3] However, the involved Faradaic reaction mainly takes place on the atoms near the surface of the used electrode materials, which results in much lower specific capacitance than lithium ion batteries.[4,5] To improve the availability of atoms, researchers have applied a series of oxide nanosheets with atomical thickness as electrodes of supercapacitors lately, and theyexhibited higher capacitances than usual powder materials.[6−9] But, oxides usually have low electrical conductivity, which limits their rate capability, another key parameter of supercapacitor.[6,7] In contrast, metal sulfides have better electrical conductivity.[10−12]

Recently, monolayer MoS_2 nanosheet-based supercapacitors were reported to have operation voltage as high as 3.5 V and Coulombic efficiency of 95% due to the unique features of high conductivity and ultrathin thickness.[13,14] Furthermore, if the simple binary sulfides can be replaced by multicomponent sulfides, the facile composition control will endow a new degree of freedom to optimize the electrical conductivity and electrochemical activity through self-doping.[15] Particularly, $NiCo_2S_4$, a potential material for energy storage applications, have attracted numerous attentions because of the higher electrochemical activity and better electrochemical performances compared to the monometal sulfides.[16,17] In addition, it is reported to have at least 2 orders of magnitude higher conductivity than that of $NiCo_2O_4$, which is beneficial to capacitive performances.[10] Up to date, various nanostructures were prepared, such as hollow spheres,[3] nanotubes,[18] nanoplates[19] and so on. However, such mixed metal sulfide nanosheets with ultrathin thickness, high conductivity and abundant pores, which are expected to improve the density of active sites, the electron transferring and ion diffusing abilities, respectively, are seldom reported.

Here, for the first time, we report on nickel–cobalt sulfide nanosheets with ultrathin thickness and nanoscale pores for supercapacitors with both high specific capacitance and excellent rate capability. A method combining lamellar micelle template growth and subsequent sulfuration was developed to high-yield fabricate nickel–cobalt sulfide nanosheets. The synergistic contributions from high density of active sites,

Received: June 17, 2015
Accepted: August 13, 2015
Published: August 13, 2015

DOI: 10.1021/acsami.5b05400
ACS Appl. Mater. Interfaces 2015, 7, 19316−19323

rapid transfer of electrons and fast diffusion of ions lead the nanosheet-assembled supercapacitors to have a high specific capacitance of 1304 F g^{-1} at a current density of 2 A g^{-1} and an excellent rate capability of 85.6% at 20 A g^{-1}. After 6000 cycles, 93.5% of the original capacitance can be reserved at a high current density of 8 A g^{-1}. The corresponding asymmetric supercapacitors have a high energy density of 41.4 Wh/kg at a power density of 414 W/kg, suggesting their promising potential for electric vehicles.

EXPERIMENTAL SECTION

Synthesis of Ultrathin Ni−Co−OH Precursors. Typically, 1.164 g of $Co(NO_3)_2{\cdot}6H_2O$, 0.5816 g of $Ni(NO_3)_2{\cdot}6H_2O$, and 2 mmol of hexamethylenetetramine (HMTA) were added into the mixed solution of ethanol (52 g), distilled water (4 g), and ethylene glycol (EG, 52 mL) containing 0.8 g of F127 to form a transparent solution. After that, the above solution was aged for 24 h and transferred into a Teflon-lined stainless steel autoclave and kept at 170 °C for 2 h. Then, the products were cooled to room temperature naturally. The obtained precursors were washed with distilled water three times.

Synthesis of Ultrathin Ni−Co−S Nanosheets. The above precursors were dispersed in 125 mL of distilled water and stirred for 0.5 h. Then, 25 mL of Na_2S (10 mmol) solution was poured into the precursor, and the mixed solution was kept at 160 °C for 2, 6, and 10 h, respectively. After the solution cooled naturally, the black products were washed with ethanol and water three times and then dried at 60 °C for 24 h. The obtained samples were denoted as Ni−Co−S-2, Ni−Co−S-6, and Ni−Co−S-10, respectively.

Characterization. The crystal structures were characterized with a multipurpose Bruker D8 XRD system. The radiation source (λ = 1.5406 Å) is from a Cu Kα radiation. Morphologies were studied via field-emission scanning electron microscopy (FESEM, FEI Quanta 250). High-resolution transmission electron microscopy (HRTEM) images were obtained from FEI Tecnai G20. The specific surface area of the sample was measured from nitrogen adsorption−desorption isotherms at liquid nitrogen temperature with a Micromeritics 3Flex instrument (Norcross, GA). X-ray photoelectron spectroscopy (XPS) was conducted on ARL-9800 with a monochromatic X-ray source AlKa excitation (1486.6 eV).

Electrochemical Performance Test. The electrodes were prepared by combining active materials, polytetrafluoroethylene (PTFE) and acetylene black in a weight ratio of 80:5:15. The as-obtained slurry was coated on precleaned nickel foam. The electrode was dried at 60 °C for 12 h under vacuum and then pressured with a force of 10 MPa. The electrochemical measurements were carried out with a three-electrode system. The platinum plate was used as counter electrode and a saturated calomel electrode was used as reference electrode. Techniques including cyclic voltammetry (CV) and chronopotentiometry were applied on a electrochemical analysis system (CHI604D, Shanghai Chenhua Instrument Co., Shanghai, China). The active material loading mass is 4 mg cm^{-2} and the electrolyte used was KOH aqueous solution with a concentration of 6 mol L^{-1}. The specific capacitance (Cs, F g^{-1}) is calculated according to the charge−discharge analyses following $Cs = It/\Delta V$, where I, t, and ΔV are discharge current density (A g^{-1}), discharge time, and potential (V), respectively. Nickel foam casted with activated carbon (AC) was used as negative electrode (AC, 80 wt %; PVA, 20 wt %) in the asymmetric supercapacitor, which was pressed with above positive electrode. The solid state electrolyte was prepared with KOH and PVA (Mw: 128 000, 0.1 g mL^{-1}). The loading mass of materials on positive and negative electrode was controlled precisely based on the charge balance mechanism. Specific capacitance of the two electrode device is calculated from the CV curve according to $C = (\int IdV)/\nu mV$, where I, V, m, and ν are the current density, potential, mass of active materials, and scan rate, respectively. The energy (E) and power (P) density are obtained from the equations: $E = 1/2CV^2$, $P = E/t$, where t is the time for a sweep segment.[1]

RESULTS AND DISCUSSION

There are kinds of methods to fabricate atom scale thin nanosheets, such as mechanical and chemical exfoliation. Due to the low yield of exfoliation from bulk materials, herein, we developed a lamellar reverse micelle assisted method followed by sulfuration for the fabrication of ultrathin Ni−Co sulfide nanosheets. First of all, inverse lamellar micelles of F127 surfactant with EG are formed in ethanol/water solvent. Then, hydrated inorganic oligomers are confined inside the inverse lamellar micelles, leading to the formation of layered inorganic oligomer agglomerates. The schematic phase diagram of surfactant−water−oil systems explaining a variety of self-assembled structures is shown in Figure S1.[20] The as-formed Ni−Co hydroxide precursor, which exhibits flexible and ultrathin hieratical structure, is shown in an SEM image in Figure S2. On the basis of this precursor, we fabricated ultrathin Ni−Co sulfides via post vulcanization.

Figure 1 presents the morphologies and microstructures of the as-prepared Ni−Co sulfides (Ni−Co−S-6). Obviously, they tend to assemble themselves into a three-dimensional hierarchical structure, as shown in Figure 1a, which is very similar to graphene or other 2D materials by similar methods.[21]

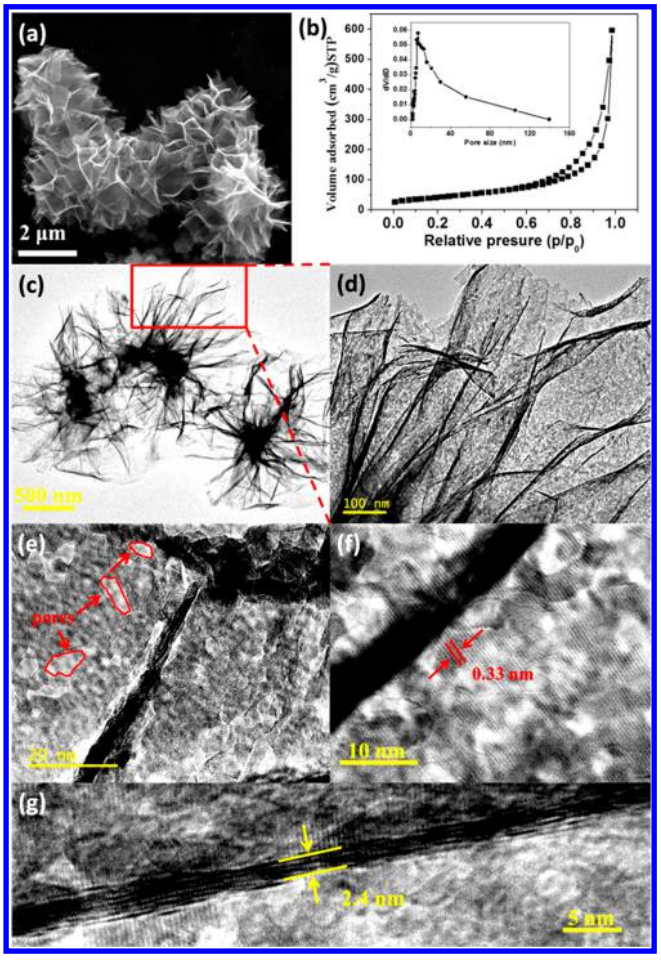

Figure 1. Ultrathin and porous features of Ni−Co sulfide nanosheets (Ni−Co−S-6). (a) SEM image of the prepared Ni−Co sulfides. (b) Nitrogen adsorption−desorption isotherms of the ultrathin Ni−Co sulfide nanosheets and (inset) Barrett−Joyner−Halenda (BJH) pore size distribution. (c−f) TEM and HRTEM images of the Ni−Co sulfides. (g) Vertical HRTEM image of Ni−Co sulfide nanosheets.

DOI: 10.1021/acsami.5b05400
ACS Appl. Mater. Interfaces 2015, 7, 19316−19323

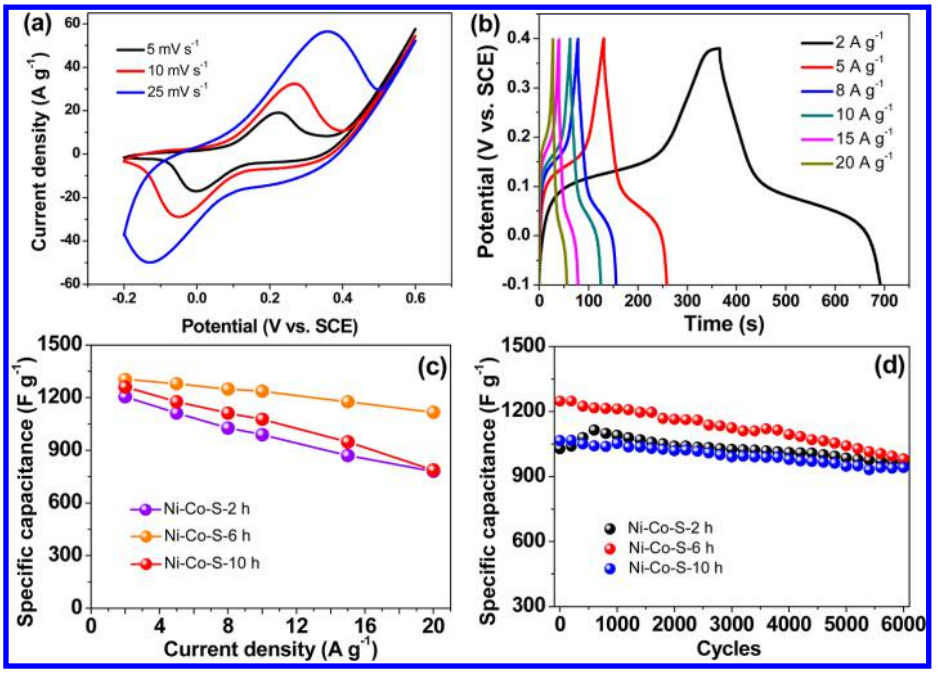

Figure 2. Electrochemical performances of Ni−Co−S nanosheets. (a) CV curves of Ni−Co−S-6 at different scanning rates. (b) Charge−discharge curves of the three samples under different current densities. (c) Specific capacitance of the three samples as a function of current density. (d) Cycling performance at 8 A g^{-1}.

The nanosheets are highly transparent under irradiation of electron beam, reflecting their ultrathin thickness, which ensures large specific surface area. The nitrogen N_2 adsorption−desorption measurements were performed to evaluate the specific surface area and pore structure of the products, as shown in Figure 1b. The isotherm profile belongs to type IV[22] and hysteresis loops are observed in the range of 0.6−1.0 P/P_0, suggesting the mesoporous feature of as-prepared sample. The Brunauer−Emmett−Teller (BET) surface area is calculated to be 141.9 m^2 g^{-1}, which is higher than that of most of the reported results for no matter oxides or sulfides.[1,23,24] The pore size distribution calculated from Barrett−Joyner−Halenda method is centered at 7.55 nm, which is an ideal pore structure for ion diffusion. From the inset in Figure 1b, most of the pores are smaller than 10 nm and some large pores are also observed due to the hierarchical structure. The combination of large surface area and mesoporosity will make great contributions to the redox reactions related energy storage.

Figure 1c−g shows the detailed TEM images of this sample. Figure 1c clearly reveals the highly flexible and transparent features of the samples, indicating the ultrathin sheetlike nanostructure, which coincides with the SEM results. The amplified image in Figure 1d further confirms the ultrathin characteristics and porosity. We can see that the sheets are composed of nanoparticles with tens of nanometers and pores formed between the spaces of nanoparticles. Most of the pores are below 10 nm with irregular shapes, as shown in Figure 1e, which is consistent with the BJH results. Additionally, strong contrast between particles and pores indicates the quasi-2D structure. Figure 1f shows the HRTEM image, and most of the particles exhibit good crystallinity. The lattice fringes with a distance of 0.33 nm correspond to (220) planes. The cross-view HRTEM image (Figure 1 g) shows that the Ni−Co sulfide is ultrathin, with a thickness of ∼2.4 nm and disordered layer structure. As far as we can confirm, Ni−Co sulfides with such thin sheets have not been achieved. In fact, the amount of any solvent in the reaction system will influence the growth of such ultrathin nanosheets greatly.[6,20] For example, when changing the amount of added water, we cannot obtain the ultrathin structures though the sheetlike morphology still remains, as shown in Figure S3. The decrease of water makes the thickness of the sheets increase, which might be attributed to the difference of solubility of surfactants. When EG was removed, only particles with mesoporous structure can be obtained.[25]

Regarding with such ultrathin nanostructure of Ni−Co sulfides, which are almost composed of surfaces with the most active sites exposed outside for the highly surface related Faradaic reactions, their potential applications in pseudocapacitors are studied systematically. Figure 2 shows the electrochemical analyses of the ultrathin Ni−Co sulfides. Figure 2a is the CV curves of Ni−Co−S-6 at different scanning rates from 5 to 25 mV s^{-1}. A pair of quasi-symmetric redox peaks can be seen in the curves, and when the scanning rate increases from 5 to 25 mV s^{-1}, the current increases, but the shape changes little. The redox peaks within the scanning range are derived from reversible Faradaic reactions including following equations according to the literatures.[26] To exclude the influence of nickel foam, CV measurements of bare nickel foam were conducted and the capacitance can be neglected compared to the samples (Figure S4).

$$CoS + OH^- \leftrightarrow CoSOH + e^- \quad (1)$$

$$NiS + OH^- \leftrightarrow NiSOH + e^- \quad (2)$$

To further investigate capacitive performance, charge−discharge measurements were conducted with a potential window of −0.1 to 0.4 V at current densities from 2 to 20 A g^{-1} (Figure 2b, Ni−Co−S-6). The specific capacitances of the samples with different vulcanizing time were calculated according to the discharge curves and the results were collected in Figure 2c as a function of current density. Impressively, all the samples exhibit capacitances higher than 1200 F g^{-1} at a

DOI: 10.1021/acsami.5b05400
ACS Appl. Mater. Interfaces 2015, 7, 19316−19323

current density of 2 A g^{-1} (detailed information can be found in Figure 4). Specially, Ni−Co−S-6 possesses higher capacitances that 1304, 1279, 1248, 1236, and 1176 F g^{-1} is obtained at the current densities of 2, 5, 8, 10, and 15 A g^{-1}. Even at a high current density of 20 A g^{-1}, it still remains 1116 F g^{-1}, 85.6% of its initial capacitance, exhibiting excellent rate capability. Interestingly, 972 F g^{-1} can still be obtained at a current density of 30 A g^{-1} (Figure S5). The electrochemical performances of the as-formed ultrathin Ni−Co hydroxide were tested, as shown in Figure S6. The C−V curves exhibit similar redox peaks and specific capacitance of 900 F g^{-1} is obtained at a current density of 2 A g^{-1}, which is high but lower than that of the Ni−Co sulfides. Besides, the electrode exhibits good rate capability and cycling stability. Considering the simple procedure without sulfuration, improvements are being carried out for the Ni−Co hydroxide nanosheets, as well as the controlling of metal ratio to achieve abundant electrochemical active sites.

It is worth noting that such a high rate capability is among the best rate performance for Ni−Co sulfides until now, as can be indexed in Table 1.[27] Most recently, Shen et al. developed

Table 1. Electrochemical Performances of Ni−Co Sulfide Electrodes in Three Electrode Systems from Recent Reports[a]

ref	capacitance	loading mass mg cm^{-2}	specific capacitance	capacitance retention
this work	**1304 F g^{-1} (2 A g^{-1})**	**4 mg cm^{-2}**	**1116 F g^{-1} at 20 A g^{-1}**	**85% from 2 to 20 A g^{-1}**
2	1036 F g^{-1} (1 A g^{-1})	5 mg cm^{-2}	705 F g^{-1} at 20 A g^{-1}	68% from 1 to 20 A g^{-1}
3	1231 F g^{-1} (2 A g^{-1})	2.3 mg cm^{-2}	877 F g^{-1} at 20 A g^{-1}	71% from 2 to 20 A g^{-1}
9	1149 F g^{-1} (1 A g^{-1})	2−3 mg cm^{-2}	888 F g^{-1} at 20 A g^{-1}	66.2% from 1 to 20 A g^{-1}
11	895.2 F g^{-1} (1 A g^{-1})	1 mg cm^{-2}	585 F g^{-1} at 20 A g^{-1}	65% from 1 to 20 A g^{-1}
17	1451 F g^{-1} (3 A g^{-1})	not reported	760 F g^{-1} at 20 A g^{-1}	52% from 3 to 20 A g^{-1}
19	437 F g^{-1} (1 A g^{-1})	not reported	231 F g^{-1} at 20 A g^{-1}	53% from 1 to 20 A g^{-1}
23	933 F g^{-1} (1 A g^{-1})	4−6 mg cm^{-2}	550 F g^{-1} at 5 A g^{-1}	50% from 0.2 to 5 A g^{-1}
27	1418 F g^{-1} (5 A g^{-1})	**0.8 mg cm^{-2}**	1285 F g^{-1} at 100 A g^{-1}	**91% from 5 to 100 A g^{-1}**
30	783 F g^{-1} (2 A g^{-1})	4.2 mg cm^{-2}	608 F g^{-1} at 15 A g^{-1}	78% from 2 to 15 A g^{-1}
35	1440 F g^{-1} (3 A g^{-1})	**not reported**	840 F g^{-1} at 20 A g^{-1}	**86.8% from 2 to 20 A g^{-1}**

[a]Results reported here are among the best performances from the aspect of rate capability, except for one work with low loading mass and in situ growth structure.

nickel−cobalt sulfide ball-in-ball and 3D $NiCo_2S_4$/carbon foam structures with remarkable performances;[2,3] 68% and 71% of the initial capacitance were obtained at a current density of 20 A g^{-1}. But, the sample here exhibits a better rate capability due to the unique ultrathin and mesoporous nanostructure and high electrical conductivity. Considering the importance of cycling stability for practical applications, the continuous charge−discharge performances were measured for 6000 cycles under a current density of 8 A g^{-1}, as shown in Figure 2c. The electrodes exhibit outstanding cycling performance, and 78.6% of its initial capacitance is obtained for Ni−Co−S-6.

As discussed above, it is easy to optimize the electrical conductivity and electrochemical activity through self-doping due to the coexistence of different elements with varied chemical valence states. Besides, crystallinity also plays an important role that amorphous electrochemically active materials usually possess better cycling stability because activation process is needed at the first several hundreds of cycles.[28] Amorphous structure can also endure the large structural changes during redox reactions well, leading to better cycling stability. Then, the effects of self-doping and crystallinity are optimized through changing the vulcanizing time. Figure S7 shows the SEM and TEM images of these two samples, both of which exhibit ultrathin and porous features with clear lattice fringes. As shown in Figure 2d, 93.4 and 88.3% of their initial capacitances were obtained for Ni−Co−S-2 and 10, respectively (Figures S8 and S9). The capacitance of Ni−Co−S-2 gradually increases after 600 cycles. It indicates that at least an additional 600 cycles are needed to fully activate the electrode. The high retention for Ni−Co−S-2 is fascinating, which is comparable with some best oxide electrode materials.

To understand the mechanism of the performance differences, we first conducted XRD measurements, as shown in Figure 3a. All the diffraction peaks can be indexed to cubic $NiCo_2S_4$ phase (JCPDS card No. 43-1477). No obvious impurity phase can be observed, indicating the total conversion of hydroxide precursor to the $NiCo_2S_4$ phase. With the extension of vulcanizing time, the crystallinity becomes better. Poorer crystallinity of Ni−Co−S-2 results in higher retention but worse electrical conductivity, which might be the reason for the lower specific capacitance compared to Ni−Co−S-6. The electrical properties of the samples were evaluated with AC impedance measurement, as shown in Figure S10. Ni−Co−S-6 exhibits the smallest resistance and the slope in low frequency region is larger than other two samples, which is consistent with the better electrochemical performances. The smallest internal resistance (IR) drops under different current densities also confirms the results (Figure S11). Besides, the smallest slope of Ni−Co−S-6 is consistent with the outstanding rate capability.

Commonly, better crystallinity ensures good electrical conductivity. However, the sample with longer treating time possesses poorer conductivity. Mixed transition metal materials usually benefit from their varied valences for the applications in energy storage devices.[29,30] For example, $NiCo_2O_4$ possesses high conductivity at 300 K due to the presence of mixed valence states.[29] With regarding to this point, we carried out X-ray photoelectron spectroscopy (XPS) and EDX measurements to analyze the chemical states inside the ultrathin Ni−Co sulfide nanosheets (Figure S12). Though all the samples can be well indexed to the structure of $NiCo_2S_4$ without any residuals and contaminants, the results of EDX indicate the deviation of the molar ration of Co/Ni. As shown in Table S1, the Co/Ni molar ratios of all the three samples are about 1.2, which is inconsistent with initial precursors. Such a difference derives from the different reaction activities of nickel and cobalt ions.[31] On the other hand, the molar ratio of S/Ni is about 2, which is also different from that in precursors. It seems that the molecular formula can be written as $NiCo_{1.2}S_2$. Figure 3b,c shows the high-resolution Ni 2p and Co 2p XPS spectra of Ni−Co−S-6. Using Gaussian fitting method, the Ni 2p spectrum is well fitted with two spin−orbit doublets and two satellite peaks. Similar results are obtained from the Co 2p spectrum. Figure 3d shows the spectrum of the S 2p region, and the two peaks at the binding energies of 161.5 and 162.7 eV are attributed to S

DOI: 10.1021/acsami.5b05400
ACS Appl. Mater. Interfaces 2015, 7, 19316−19323

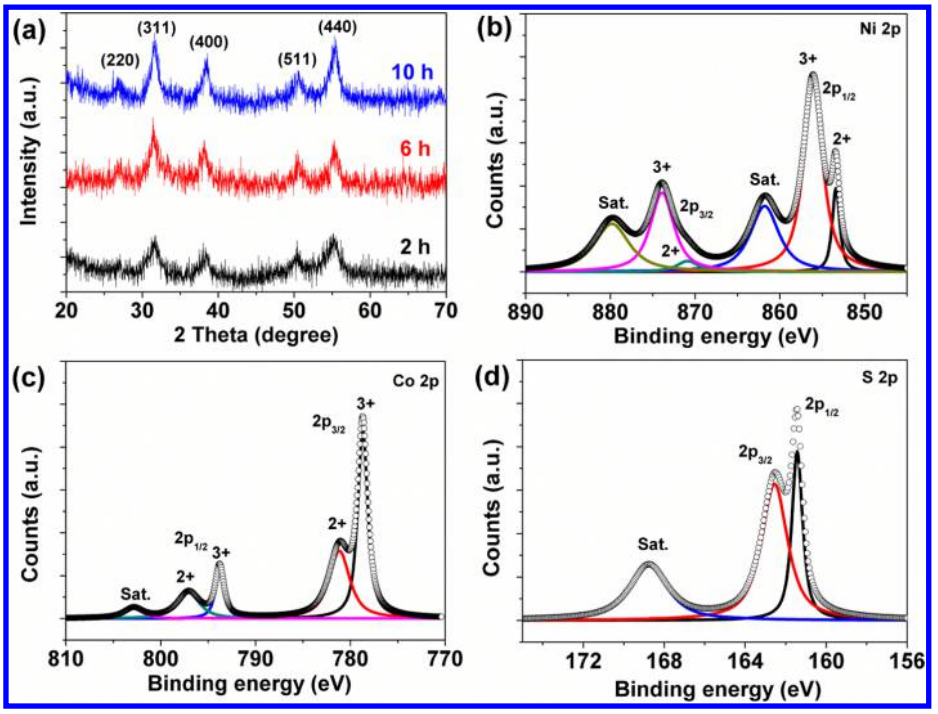

Figure 3. Crystallography and chemical states of Ni–Co–S nanosheets. (a) XRD patterns of samples with different vulcanizing time. High-resolution XPS spectra of (b) Ni 2p, (c) Co 2p, and (d) S 2p for Ni–Co–S-6.

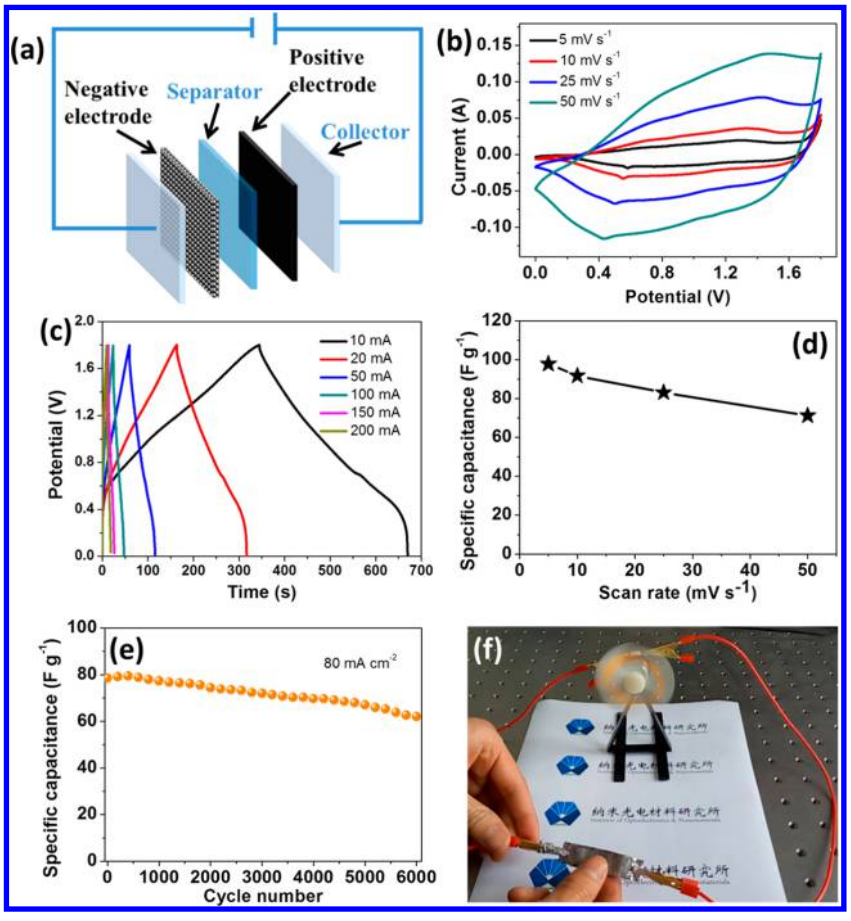

Figure 4. Electrochemical performance of Ni–Co–S/AC asymmetric supercapacitor. (a) The schematic illustration of the asymmetric supercapacitor based on the ultrathin Ni–Co sulfide nanosheets and activated carbon. (b) CV and (c) calculated specific capacitance as a function of scan rate. (d) Charge–discharge curves of the asymmetric supercapacitor. (e) Cycling stability of the full cell. (f) A picture showing a rotating motor derived by one cell.

DOI: 10.1021/acsami.5b05400
ACS Appl. Mater. Interfaces 2015, 7, 19316–19323

$2p_{1/2}$ and S $2p_{3/2}$, respectively. The XPS analyses of other two samples are shown in Figures S13 and S14. Then we can conclude that the ultrathin nanosheets contain Ni^{2+}, Ni^{3+}, Co^{2+}, Co^{3+}, and S^{2-}, which agrees well with previous reports.[17,32,33] But, the molar ratios of Co/Ni decrease to ~0.57, according to the survey spectra, which are almost the reverse of the precursor, as shown in Table S1. It means that the surface possesses totally different chemical states compared to the inside part because of the ultrathin structure.

Despite the different chemical states at the surface and inside and the presence of varied valences for both of the transition metal elements, the ultrathin nanosheets still keep the crystal structure of $NiCo_2S_4$. Then, we can conclude that most of the Ni and Co occupies the sites where they should be. Herein, we propose a concept of self-doping related to the mixed valence states to explain the interesting phenomenon referring to chemical states and conductivity. Theoretically, the presence of Ni^{3+} will provide extra electrons as n-type doping while the presence of Co^{2+} will result in extra holes as p-type doping. Therefore, more Ni^{3+} and Co^{3+} will lead to higher electrical conductivity for electrons and better electrochemical performance.[34] The detailed analyses according to the Ni 2p and Co 2p XPS spectra are shown in Figure S15 that Ni^{3+} decreases with the increase of vulcanizing time. On the other hand, the percentage of Co^{3+} in Ni−Co−S-6 is higher than that in the other two samples, indicating better electrical conductivity. A greater percentage of Ni^{3+} formed during the first hydrothermal reactions because of its high reactivity, while it decreased during sulfuration. For Co^{3+}, the percent was not very high at first and oxidized with short heating treatment but reduced with longer time sulfuration. The reduction of Ni^{3+} and Co^{3+} can be attributed to the formation of H_2S during hydrothermal reactions, which possess high reducibility. Obviously, transportation of electrons at the surface is more difficult for Ni−Co−S-10 because this sample possess the lowest percent of Ni^{3+} and Co^{3+}. Most of the electrons transmit through the surface between adjacent particles, and then transfer to the current collectors. Good surface electrical conductivity will lead to higher capacitance and better rate capability. Therefore, Ni−Co−S-6 possesses the best rate capability due to good electrical conductivity resulted from good crystallinity and optimized self-doping. In contrast, Ni−Co−S-10 exhibits worse performance due to low conductivity even though it has better crystallinity.

To further investigate the capacitive performance of the ultrathin Ni−Co sulfide nanosheets for practical applications, we fabricated asymmetric supercapacitors using Ni−Co−S-6 and activated carbon (AC) as the positive and negative electrodes with a piece of cellulose paper as the separator according to the literature (Figure 4a).[35] The mass of active material and AC was controlled according to the principle of charge balance at a scanning rate of 25 mV s^{-1} in a three-electrode system. The compared CV curves are shown in Figure S16 and the mass for active materials and activated carbon are about 3.8 and 18 mg cm^{-2}, respectively. Referring to previous reports, the AC can exhibit a typical characteristic of electric double-layer capacitance in KOH aqueous solution within the range of −1.2 to 0 V.[35] Then, the working voltage of the assembled device is expected to be 1.8 V.

Figure 4b shows the CV curves of the full cell within a voltage of 0−1.8 V. It is worth noting that there is no obvious oxygen evolution. Such high working voltage is almost twice that of conventional AC based symmetric supercapacitors. Both of the active materials and AC contribute to the capacitance and with the increase of scanning rate from 5 to 100 mV s^{-1}, no obvious change was observed for shapes of the CV curves, indicating the fast charge−discharge performance of the device. The calculated specific capacitances as a function of scanning rate are plotted in Figure 4c. The specific capacitance of the device is 92 F g^{-1} at 5 mV s^{-1} and 57.4% of its initial capacitance is retained when the scan rate increases to 100 mV s^{-1}. Charge−discharge performance under different current densities is also illustrated in Figure 4d, and the usual discharge plateau in three-electrode system disappears. Figure 4e exhibits the long-term cycling stability at a current density of 80 mA cm^{-2}, and the device still retain 79.1% of its original capacitance, which agrees well with the half-cell results in three-electrode system. Additionally, the overlap of electrochemical impedance spectroscopy curves implies the high stability of the asymmetric supercapacitor (Figure S17). Strikingly, a single cell can drive a motor robustly after seconds of charging, as shown in Figure 4f.

The energy density and power density of the asymmetric supercapacitor device is shown in Figure 5. We also compare

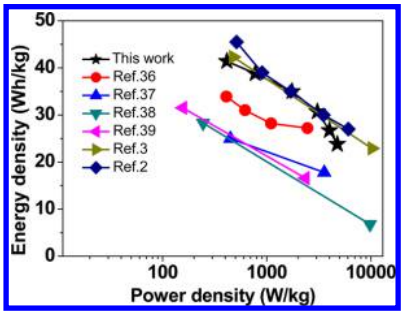

Figure 5. Ragone plots of the asymmetric supercapacitors and performances of references.

the values with other high performance devices (the same material, Ni−Co sulfide) from recent reports.[2,3,36−39] The energy density decreases from 41.4 to 23.8 Wh/kg when power density increases from 414 W/kg to 4.8 kW/kg. Though just commercial activated carbon is used as negative electrode material, performance of the asymmetric supercapacitor in this work is among the best devices from the very recent reports. In fact, the performance of such ASCs is limited by negative material. If the electrochemical performance of negative material is improved, higher energy density will be obtained with higher power density. Anyway, the ultrathin and 3D porous nanostructure of the Ni−Co sulfides makes great contributions to the outstanding capacitive performances.

CONCLUSION

In summary, ultrathin Ni−Co sulfide nanosheets are synthesized successfully to make the best of all the atoms. A specific surface area of 141.9 m^2 g^{-1} is obtained, and the synergistic effects of high specific surface area, 3D mesoporous nanostructure, and high electrical conductivity make great contributions to the capacitive performance. Consequently, a specific capacitance of 1304 F g^{-1} is obtained at a current density of 2 A g^{-1} with excellent rate capability. We can control the crystallinity of the ultrathin nanosheets precisely to achieve prominent cycling stability (93.4%) at a high current density (8 A g^{-1}). Besides, a concept of self-doping is introduced to explain the interesting relationship between crystallinity and inside chemical structure. An asymmetric supercapacitor has

DOI: 10.1021/acsami.5b05400
ACS Appl. Mater. Interfaces 2015, 7, 19316−19323

been fabricated successfully with high energy and power density and exhibits remarkable cycling stability. This work provides a promising electrode material for next-generation energy storage devices and catalysis.

■ ASSOCIATED CONTENT

Supporting Information

The Supporting Information is available free of charge on the ACS Publications website at DOI: 10.1021/acsami.5b05400.

SEM, XPS, and detailed electrochemical results (PDF)

■ AUTHOR INFORMATION

Corresponding Author

*E-mail: zeng.haibo@njust.edu.cn.

Author Contributions

§These authors contributed equally.

Notes

The authors declare no competing financial interest.

■ ACKNOWLEDGMENTS

This work is financially supported by the National Basic Research Program of China (grant number 2014CB931700), NSFC (grant number 61222403), and the Priority Academic Program Development of Jiangsu Higher Education Institutions.

■ REFERENCES

(1) Li, X. M.; Jiang, L.; Zhou, C.; Liu, J.; Zeng, H. B. Integrating Large Specific Surface Area and High Conductivity in Hydrogenated NiCo2O4 Double-shell Hollow Spheres to Improve Supercapacitors. *NPG Asia Mater.* **2015**, *7*, e165.

(2) Shen, L. F.; Wang, J.; Xu, G. Y.; Li, H. S.; Dou, H.; Zhang, X. G. $NiCo_2S_4$ Nanosheets Grown on Nitrogen-Doped Carbon Foams as an Advanced Electrode for Supercapacitors. *Adv. Energy Mater.* **2015**, *5*, 1400977.

(3) Shen, L. F.; Yu, L.; Wu, H. B.; Yu, X. Y.; Zhang, X. G.; Lou, X. W. Formation of Nickel Cobalt Sulfide Ball-in-ball Hollow Spheres with Enhanced Electrochemical Pseudocapacitive Properties. *Nat. Commun.* **2015**, *6*, 6694.

(4) Xiao, X. C.; Zhou, W. D.; Kim, Y. N.; Ryu, I.; Gu, M.; Wang, C. M.; Liu, G.; Liu, Z. Y.; Gao, H. J. Regulated Breathing Effect of Silicon Negative Electrode for Dramatically Enhanced Performance of Li-Ion Battery. *Adv. Funct. Mater.* **2015**, *25*, 1426−1433.

(5) Liu, N.; Lu, Z. D.; Zhao, J.; McDowell, M. T.; Lee, H. W.; Zhao, W. T.; Cui, Y. A Pomegranate-inspired Nanoscale Design for Large-volume-change Lithium Battery Anodes. *Nat. Nanotechnol.* **2014**, *9*, 187−192.

(6) Zhu, Y. Q.; Cao, C. B.; Tao, S.; Chu, W. S.; Wu, Z. Y.; Li, Y. D. Ultrathin Nickel Hydroxide and Oxide Nanosheets: Synthesis, Characterizations and Excellent Supercapacitor Performances. *Sci. Rep.* **2014**, *4*, 5787.

(7) Fan, Y. Q.; Shao, G. J.; Ma, Z. P.; Wang, G. L.; Shao, H. B.; Yan, S. Ultrathin Nanoflakes Assembled 3D Hierarchical Mesoporous Co_3O_4 Nanoparticles for High-Rate Pseudocapacitors. *Part. Part. Syst. Charact.* **2014**, *31*, 1079−1083.

(8) Feng, C.; Zhang, J. F.; He, Y.; Zhong, C.; Hu, W. B.; Liu, L.; Deng, Y. D. Sub-3 nm Co_3O_4 Nanofilms with Enhanced Supercapacitor Properties. *ACS Nano* **2015**, *9*, 1730−1739.

(9) Zhao, J. H.; Zheng, M. B.; Run, Z.; Xia, J.; Sun, M. J.; Pang, H. 1D $Co_{2.18}Ni_{0.82}Si_2O_5(OH)_4$ Architectures Assembled by Ultrathin Nanoflakes for High-performance Flexible Solid-state Asymmetric Supercapacitors. *J. Power Sources* **2015**, *285*, 385−392.

(10) Chen, H. C.; Jiang, J. J.; Zhang, L.; Wan, H. Z.; Qi, T.; Xia, D. D. Highly Conductive $NiCo_2S_4$ Urchin-like Nanostructures for High-rate Pseudocapacitors. *Nanoscale* **2013**, *5*, 8879−8883.

(11) Yu, L.; Zhang, L.; Wu, H. B.; Lou, X. W. Formation of $Ni_xCo_{3-x}S_4$ Hollow Nanoprisms with Enhanced Pseudocapacitive Properties. *Angew. Chem., Int. Ed.* **2014**, *53*, 3711−3714.

(12) Gao, Y.; Mi, L. W.; Wei, W. T.; Cui, S. Z.; Zheng, Z.; Hou, H. W.; Chen, W. H. Double Metal Ions Synergistic Effect in Hierarchical Multiple Sulfide Microflowers for Enhanced Supercapacitor Performance. *ACS Appl. Mater. Interfaces* **2015**, *7*, 4311−4319.

(13) Xiao, J. W.; Wan, L.; Yang, S. H.; Xiao, F.; Wang, S. Design Hierarchical Electrodes with Highly Conductive $NiCo_2S_4$ Nanotube Arrays Grown on Carbon Fiber Paper for High-Performance Pseudocapacitors. *Nano Lett.* **2014**, *14*, 831−838.

(14) Liu, Y.; Zhang, J. N.; Wang, S. P.; Wang, K. X.; Chen, Z. M.; Xu, Q. Facilely Constructing 3D Porous $NiCo_2S_4$ Nanonetworks for High-performance Supercapacitors. *New J. Chem.* **2014**, *38*, 4045−4048.

(15) Xu, Y. X.; Lin, Z. Y.; Zhong, X.; Huang, X. Q.; Weiss, N. O.; Huang, Y.; Duan, X. F. Holey Graphene Frameworks for Highly Efficient Capacitive Energy Storage. *Nat. Commun.* **2014**, *5*, 5554.

(16) Du, W. M.; Wang, Z. Y.; Zhu, Z. Q.; Hu, S.; Zhu, X. Y.; Shi, Y. F.; Pang, H.; Qian, X. F. Facile Synthesis and Superior Electrochemical Performances of $CoNi_2S_4$/Graphene Nanocomposite Suitable for Supercapacitor Electrodes. *J. Mater. Chem. A* **2014**, *2*, 9613−9619.

(17) Pu, J.; Wang, T. T.; Wang, H. Y.; Tong, Y.; Lu, C. C.; Kong, W.; Wang, Z. H. Direct Growth of $NiCo_2S_4$ Nanotube Arrays on Nickel Foam as High-Performance Binder-Free Electrodes for Supercapacitors. *ChemPlusChem* **2014**, *79*, 577−583.

(18) Cai, D. P.; Wang, D. D.; Wang, C. X.; Liu, B.; Wang, L. L.; Liu, Y.; Li, Q. H.; Wang, T. H. Construction of Desirable $NiCo_2S_4$ Nanotube Arrays on Nickel Foam Substrate for Pseudocapacitors with Enhanced Performance. *Electrochim. Acta* **2015**, *151*, 35−41.

(19) Pu, J.; Cui, F. L.; Chu, S. B.; Wang, T. T.; Sheng, E. H.; Wang, Z. H. Preparation and Electrochemical Characterization of Hollow Hexagonal $NiCo_2S_4$ Nanoplates as Pseudocapacitor Materials. *ACS Sustainable Chem. Eng.* **2014**, *2*, 809−815.

(20) Sun, Z. Q.; Liao, T.; Dou, Y. H.; Hwang, S. M.; Park, M.-S.; Jiang, L.; Kim, J. H.; Dou, S. X. Generalized Self-assembly of Scalable Two-dimensional Transition Metal Oxide Nanosheets. *Nat. Commun.* **2014**, *5*, 3813.

(21) Xie, X. Q.; Ao, Z. M.; Su, D. W.; Zhang, J. Q.; Wang, G. X. MoS_2/Graphene Composite Anodes with Enhanced Performance for Sodium-Ion Batteries: The Role of the Two-Dimensional Heterointerface. *Adv. Funct. Mater.* **2015**, *25*, 1393−1403.

(22) Yuan, C. Z.; Li, J. Y.; Hou, L. R.; Lin, J. D.; Pang, G.; Zhang, L. H.; Lian, L.; Zhang, X. G. Template-engaged Synthesis of Uniform Mesoporous Hollow $NiCo_2O_4$ Sub-microspheres Towards High-performance Electrochemical Capacitors. *RSC Adv.* **2013**, *3*, 18573−18578.

(23) Peng, S. J.; Li, L. L.; Li, C. C.; Tan, H. T.; Cai, R.; Yu, H.; Mhaisalkar, S.; Srinivasan, M.; Ramakrishna, S.; Yan, Q. Y. In Situ Growth of $NiCo_2S_4$ Nanosheets on Graphene for High-performance Supercapacitors. *Chem. Commun.* **2013**, *49*, 10178−10180.

(24) Zhang, Y. F.; Ma, M. Z.; Yang, J.; Sun, C. C.; Su, H. Q.; Huang, W.; Dong, X. C. Shape-controlled Synthesis of $NiCo_2S_4$ and Their Charge Storage Characteristics in Supercapacitors. *Nanoscale* **2014**, *6*, 9824−9830.

(25) Hsu, H. Y.; Chang, K. H.; Salunkhe, R. R.; Hsu, C. T.; Hu, C. C. Synthesis and Characterization of Mesoporous Ni−Co Oxy-hydroxides for Pseudocapacitor Application. *Electrochim. Acta* **2013**, *94*, 104−112.

(26) Wan, H. Z.; Jiang, J. J.; Yu, J. W.; Xu, K.; Miao, L.; Zhang, L.; Chen, H. C.; Ruan, Y. J. $NiCo_2S_4$ Porous Nanotubes Synthesis via Sacrificial Templates: High-performance Electrode Materials of Supercapacitors. *CrystEngComm* **2013**, *15*, 7649−7651.

(27) Chen, W.; Xia, C.; Alshareef, H. N. One-Step Electrodeposited Nickel Cobalt Sulfide Nanosheet Arrays for High-Performance Asymmetric Supercapacitors. *ACS Nano* **2014**, *8*, 9531−9541.

(28) Li, H. B.; Gao, Y. Q.; Wang, C. X.; Yang, G. W. A Simple Electrochemical Route to Access Amorphous Mixed-Metal Hydroxides for Supercapacitor Electrode Materials. *Adv. Energy Mater.* **2015**, *5*, 1401767.

DOI: 10.1021/acsami.5b05400
ACS Appl. Mater. Interfaces 2015, 7, 19316−19323

(29) Hu, L. F.; Wu, L. M.; Liao, M. Y.; Hu, X. H.; Fang, X. S. Electrical Transport Properties of Large, Individual $NiCo_2O_4$ Nanoplates. *Adv. Funct. Mater.* **2012**, *22*, 998−1004.
(30) Yuan, C. Z.; Zhang, L. H.; Hou, L. R.; Pang, G.; Zhang, X. G. Green Template-Free Synthesis of Mesoporous Ternary CoNi−Mn Oxide Nanowires Towards High-Performance Electrochemical Capacitors. *Part. Part. Syst. Character.* **2014**, *31*, 778−787.
(31) Wang, X.; Yan, C.; Sumboja, A.; Lee, P. S. High Performance Porous Nickel Cobalt Oxide Nanowires for Asymmetric Supercapacitor. *Nano Energy* **2014**, *3*, 119−126.
(32) Peng, T.; Qian, Z. Y.; Wang, J.; Song, D. L.; Liu, J. Y.; Liu, Q.; Wang, P. Construction of Mass-controllable Mesoporous $NiCo_2S_4$ Electrodes for High Performance Supercapacitors. *J. Mater. Chem. A* **2014**, *2*, 19376−19382.
(33) Sun, M.; Tie, J. J.; Cheng, G.; Lin, T.; Peng, S. M.; Deng, F. Z.; Ye, F.; Yu, L. In Situ Growth of Burl-like Nickel Cobalt Sulfide on Carbon Fibers as High-performance Supercapacitors. *J. Mater. Chem. A* **2015**, *3*, 1730−1736.
(34) Wang, X.; Yan, C.; Sumboja, A.; Yan, J.; Lee, P. S. Achieving High Rate Performance in Layered Hydroxide Supercapacitor Electrodes. *Adv. Energy Mater.* **2014**, *4*, 1301240.
(35) Zhou, C.; Zhang, Y. W.; Li, Y. Y.; Liu, J. P. Construction of High-Capacitance 3D CoO@Polypyrrole Nanowire Array Electrode for Aqueous Asymmetric Supercapacitor. *Nano Lett.* **2013**, *13*, 2078−2085.
(36) Hu, W.; Chen, R. Q.; Xie, W.; Zou, L.; Qin, N.; Bao, D. H. $CoNi_2S_4$ Nanosheet Arrays Supported on Nickel Foams with Ultrahigh Capacitance for Aqueous Asymmetric Supercapacitor Applications. *ACS Appl. Mater. Interfaces* **2014**, *6*, 19318−19326.
(37) Li, Y. H.; Cao, L. J.; Qiao, L.; Zhou, M.; Yang, Y.; Xiao, P.; Zhang, Y. H. Ni-Co Sulfide Nanowires on Nickel Foam with Ultrahigh Capacitance for Asymmetric Supercapacitors. *J. Mater. Chem. A* **2014**, *2*, 6540−6548.
(38) Zhu, Y. R.; Wu, Z. B.; Jing, M. J.; Yang, X. M.; Song, W. X.; Ji, X. B. Mesoporous NiCo2S4 Nanoparticles as High-performance Electrode Materials for Supercapacitors. *J. Power Sources* **2015**, *273*, 584−590.
(39) Chen, H. C.; Jiang, J. J.; Zhang, L.; Xia, D. D.; Zhao, Y. D.; Guo, D. Q.; Qi, T.; Wan, H. Z. In Situ Growth of $NiCo_2S_4$ Nanotube Arrays on Ni Foam for Supercapacitors: Maximizing Utilization Efficiency at High Mass Loading to Achieve Ultrahigh Areal Pseudocapacitance. *J. Power Sources* **2014**, *254*, 249−257.

DOI: 10.1021/acsami.5b05400
ACS Appl. Mater. Interfaces 2015, 7, 19316−19323